Full length article

An automated early diabetic retinopathy detection through improved blood vessel and optic disc segmentation

Shailesh Kumar[a], Abhinav Adarsh[a], Basant Kumar[a], Amit Kumar Singh[b],*

[a] ECED, MNNIT Allahabad, Prayagraj, India
[b] CSED, NIT Patna, Patna, India

HIGHLIGHTS

- Presents an automated early diabetic retinopathy detection scheme for colour fundus image.
- Uses mathematical morphology operation for pre-processing and blood vessel detection.
- The accuracy of the proposed algorithm is evaluated based on sensitivity and specificity.
- The method offer better performance than similar stat-of-the-art techniques.

ARTICLE INFO

ABSTRACT

This paper presents an automated early diabetic retinopathy detection scheme from color fundus images through improved segmentation strategies for optic disc and blood vessels. The red lesions, microaneurysms and hemorrhages are the earliest signs of diabetic retinopathy. This paper essentially proposes improved techniques for microaneurysm as well as hemorrhages detection, which eventually contribute in the overall improvement in the early detection of diabetic retinopathy. The proposed method consists of five stages- pre-processing, detection of blood vessels, segmentation of optic disc, localization of fovea, feature extraction and classification. Mathematical morphology operation is used for pre-processing and blood vessel detection. Watershed transform is used for optic disc segmentation. The main contribution of this model is to propose an improved blood vessel and optic disc segmentation methods. Radial basis function neural network is used for classification of the diseases. The parameters of radial basis function neural network are trained by the features of microaneurysm and hemorrhages. The accuracy of the proposed algorithm is evaluated based on sensitivity and specificity, which are 87% and 93% respectively.

1. Introduction

The aim of mass screening programs for diabetic retinopathy is to detect and diagnose the disorder earlier than it causes loss of vision. Mass screening programs use computerized fundus photography of retina with or without mydriasis (pupil dilation) to detect eye diseases. Automated analysis of retinal pictures has the likelihood to enhance the effectiveness of screening programs in comparison to manual picture evaluation. Diabetic Retinopathy (DR) is an eye retinal disease caused by long standing diabetic condition also referred as diabetic mellitus (DM) [1,2,3]. DR is a vital cause of blindness in the functioning age population between 20 and 60 years. There is 78% chance of having DR if the patient is above 30 years of age and suffers from diabetes for more than 15 years [1,4].

Because of diabetic retinopathy, multiple lesions are produced on retinal surface. Microaneurysms, hemorrhages, exudates, and cotton wools are the major lesions, which indicate the presence of DR. *Microaneurysms* (MAs) are the lesions that appear at the premature phase of the disease and the number of MAs grow as disease develops [5,6]. *Hemorrhages* are likely to be the lesions that appear after MAs. Hemorrhages appear in case of blood leakage from the vascular tree present in the retina [7,8]. Hence, the detection of MAs and hemorrhages plays important role in automated retinopathy detection at early stages [9,10,11]. At later stages, yellow- white colour plasma starts leaking from blood capillaries, known as *hard exudates* [12]. *Cotton wools* appear next to exudates, which are silver color contusions caused

---

by fats outpouring from veins. MAs, hemorrhages and exudates are the features of non-proliferative diabetic retinopathy (NDPR). NDPR is an early stage of diabetic retinopathy. The advance stage of DR is known as proliferative diabetic retinopathy (PDR) [13,14]. In this stage, the main blood vessels of retina are completely blocked. In order to supply oxygen to retina, new blood vessels grow, named as abnormal blood vessels [15,16]. The vision of patient is severely affected in PDR. The fundamental problem with DR is asymptomatic, it does not affect the vision until it reaches at advance stage. DR may affect one or both eyes simultaneously.

A retinal color fundus image contains a variety of structures such as vascular tree, optic disc, fovea and red lesions, like MAs and hemorrhages. MAs and hemorrhages are considered as dark lesions, whereas exudates and cotton wools are considered as bright lesions. In order to detect lesions from the fundus image, firstly we have to remove the morphological structures present inside the retina. Mathematical morphological operation is used for detection of vascular tree, segmentation of optic disc and localization of fovea. Morphology is a branch of science that studies the shape and structure of creatures and plants. Morphology operation is a non-linear image processing technique [17].

Morphological processing commonly consists of two parts: objective image and structuring element. The size of structuring element is very small as compared to objective image. The structuring element is made of 0′s and 1′s and the shape of structuring element could be flat such as linear, disc, square, diamond shape and non-flat such as ball shape. The structuring element can be placed inside the concerning image if it fits, and outside if it does not fit. The structural information is derived by identifying the location at which the structuring element fits inside the picture. It depends upon size and shape of structuring element [18,19]. Details of morphology operation is discussed in later section. In this paper, mathematical morphology is widely used for pre-processing and extraction of vascular tree, optic disc and fovea. We have used mathematical morphology operation which is iterated one more time, in order to get improved blood vessels segmentation. Optic disc segmentation is done using Watershed Transform.

After the removal of all morphological structures the retinal fundus image under investigation is left with white spots of nearly circular shape. These structures are described as MAs and hemorrhages. In the next stage, seven features (area, perimeter, circularity, number of objects, major axis, minor axis, aspect ratio) are extracted from MAs and hemorrhages: these features are used for training a classification model for automated detection of DR. Radial Basis Function Neural Network (RBFNN) is utilized as classification model. RBFNN is a special type of neural network which consists of only three layers, including input and output layer. The developed neural network model classifies the fundus image into healthy image and DR image. The proposed DR detection scheme is exploiting the combined benefits of morphology operation (for blood vessel segmentation), Watershed Transformation (Optic disc segmentation) and RBF NN (for DR classification). Overall contribution of the proposed work can be summarized as follows:

1. To propose an improved blood vessels detection technique by morphological iterative process
2. To develop an automated Optic Disc algorithm using marker controlled Watershed Transform
3. Implementation of RBFNN based classification mass screening of diabetic retinopathy.

Rest of the paper is organized as follows. Previous works related to proposed scheme are presented in Section 2. Proposed schemes for microaneurysm and hemorrhages detection from fundus images are described in Section 3. Results and conclusions are explained in Sections 4 and 5 respectively.

2. Previous related work

Automated detection of eye related diseases from fundus image is a hot topic for researchers these days. Automated detection of glaucoma and DR have emerged as an important topic for researchers working in the area of medical image processing and computer vision. A number of DR detection systems and algorithms have been suggested in last two decades. Several preprocessing methods of retinal fundus images have been proposed. Seyed Hossein Rasta et al. [20] and Sharad K Yadav et al. [21] have presented the comparative analysis of illumination correction and contrast enhancement methods. V. Thirilogasundari et al. [22] and Ayyaz Hussain et al. [23] have suggested fuzzy based methods for removal of impulse noise.

Literature review of some of the automated DR detection algorithms from fundus images are discussed here. Daniel Welfer et al. [24] suggested a method for detachment of optic disc in color fundus images using mathematical morphological operation. In this work, optic disc detection has been divided into two parts; First part finds the points on optic disc and second part finds the optic disc boundary. In order to find internal optic disc point, they have applied morphological operations such as 'skeletonization' and 'recursive pruning' on blood vessels. They have used the pixels of main blood vessels, which are in the vicinity of optic disc center, as 'internal marker' and circles of different diameters, centered at optic disc center point, as 'external marker'. K. Parvati et al. [25] proposed image segmentation method based on gray-scale morphology using Watershed Transform for medical images. First of all, morphological gradient is applied on gray-scale image, which shows the edge toughness of every pixel. They have created internal markers and external markers using regional maxima. These markers are superimposed with original image, followed by applying Watershed Transform for segmentation. Over segmentation is common problem of Watershed Transform. The problem arises due to noise and quantization error. Sarni Suhaila Rahim et al. [2] proposed automatic detection of microaneurysm in color fundus images for diabetic retinopathy. They explored several preprocessing, feature extraction and classification techniques. In system I, they have used adaptive histogram equalization, Discrete Wavelet Transform, filtering and morphology process for preprocessing. Area of pixels, mean and standard deviation are the extracted features of DR. In System II, shade correction, vessel segmentation and morphology operation have been used for preprocessing techniques. For classification, they have used decision tree, K-nearest neighbor, radial basis function, polynomial support vector machine. System III consists of only two stages: preprocessing and detection of microaneurysm. Preprocessing has been done by grey scale conversion and adaptive histogram equalization. Circular Hough Transform has been proposed to locate the microaneurysm due to the circular shape of microaneurysm. System IV also consists of two stages. Combination of preprocessing techniques, grey scale conversion and Contrast Limited Adaptive Histogram Equalization (CLAHE) are implemented in first system, whereas grey scale and fuzzy histogram equalization are used in second system. Circular Hough Transform is used for detection of microaneurysms. Jang Pyo Bae et al. [9] proposed a study on hemorrhage detection using hybrid method in fundus images. Detection of hemorrhages from fundus images consists of different stages such as preprocessing and candidate extraction. The objective of preprocessing is to make the brightness of picture uniform and improve the difference among hemorrhages and ground. They applied hue saturation value for brightness correction and CLAHE to fundus images. Template matching with normalized cross correlation has been used for candidate extraction. Shailesh Kumar and Basant Kumar [26] proposed a DR detection system by extracting area and number of MAs from color fundus images. The detection system consists of multiple phases namely; preprocessing, exudate detection, blood vessel extraction, optic disc segmentation, fovea localization, feature extraction and classification of fundus image. They have extracted two features namely, area and number of MAs, after extraction of MAs from retinal images.
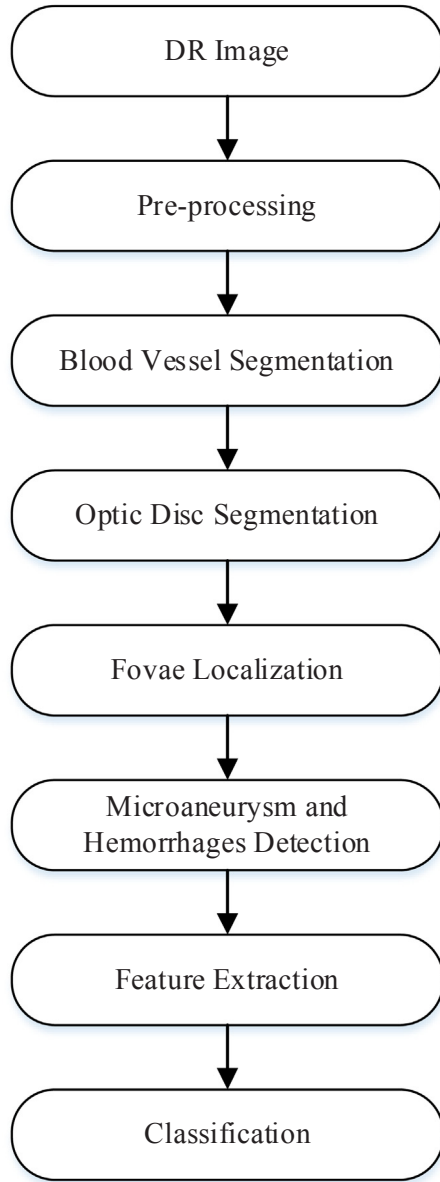
Fig. 1. Block diagram of automatic detection of DR from fundus images.

Fig. 2. (a) Resized RGB image (b) Gray image.

the literature [20]. Retinal color fundus images often suffer from non-illumination, low contrast due to anatomy of the eye fundus (the eye fundus with a 3-D concave shape), opaque media inside the eye, wide angle optics of the cameras, variation in size of pupil, geometry of sensor array, and movement of eye during capturing image. Hence, preprocessing plays important role in retinal fundus image analysis. The main objective of preprocessing technique is to increase the detection probability of disease by visual assessment and computer aided segmentation of retinal images. First of all, color fundus images, which are taken from different sources, are resized to 640 × 480 pixels. In order to reduce processing time, images are converted into gray scale. The resized image and gray scale images are shown in Fig. 2. Retinal color fundus image consists of three channels namely red, green and blue channel. Green channel of the RGB image is used for preprocessing because of the great contrast between blood vessels and background, and the best contrast between optic disc and tissue inside the retina. Red channel is moderately bright and veins of choroid is very noticeable. The retinal vessels are visible however, it shows less contrast than green channel. The gray scale image will be used in localization of optic disc. Blue channel is not used in detection because it contains more noise and less information about the morphological structure of the retina.

Some Basic Morphology Operations

Erosion: The erosion of gray scale image X by structuring element Y is symbolized by $X\theta Y$ is described as

$$X \ominus Y(p, q) = \min_{s,t \in Y}\{X(p + s, q + t)\} \tag{1}$$

where p, q, s and t are pixels values in X and Y respectively.

Dilation: It is a dual operation to erosion. It is derived from erosion by set complementation. The dilation of gray scale image X by Y is symbolized by $X \oplus Y$, is described as

$$X \oplus Y(p, q) = \max_{s,t \in Y}\{X(p - s, q - t)\} \tag{2}$$

Opening: The opening of binary image X by structuring element Y is denoted by $X°Y$ and defined as erosion followed dilation

$$X°Y = (X \ominus Y) \oplus Y \tag{3}$$

Closing: The closing operation of binary image X by structuring element Y is denoted by $X•Y$ and defined as dilation followed by erosion.

$$X•Y = (X \oplus Y) \ominus Y \tag{4}$$

Top-hat transformation: The top-hat transformation of a gray scale image I is defined as subtracting its opening from itself.

$$T_{hat}(I) = I - (I°b) \tag{5}$$

Bottom-hat transformation: The bottom-hat transformation of gray scale image is I defined as subtracting the image from its closing operation.

$$B_{hat}(I) = (I•b) - I \tag{6}$$

There are some limitations of the existing DIP based diabetic retinopathy detection methods. Some red lesions are very near to the blood vessels, making it difficult to be distinguished. Microaneurysms usually have very small size ($\leq 125\ \mu m$ of diameter) and small intensity of variation with the background, which makes the detection of microaneurysms a complicated task. The biggest challenge for the detection of red lesion is the segmentation of microaneurysms in the region of low contrast and in presence of white lesions in the retina (exudates). If one has cataract, glaucoma, macular degeneration or any other eye disease then diabetic retinopathy detection is impossible [1,2].

3. Proposed scheme for early diabetic retinopathy detection

3.1. Pre-processing of fundus image

Proposed diabetic retinopathy detection model consists of mainly three parts such as preprocessing, feature extraction and classification. The block diagram for automatic detection of DR is shown in Fig. 1. Preprocessing is the essential part of detection technique using image processing. There are variety of pre-processing methods suggested in
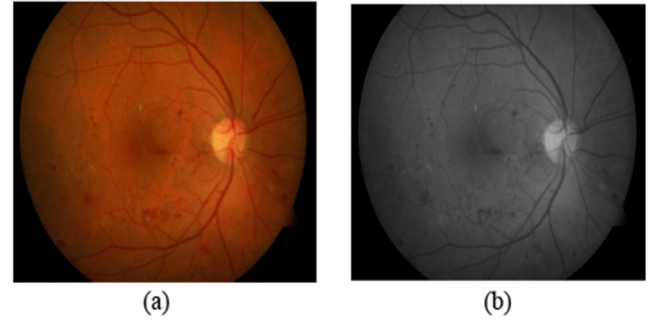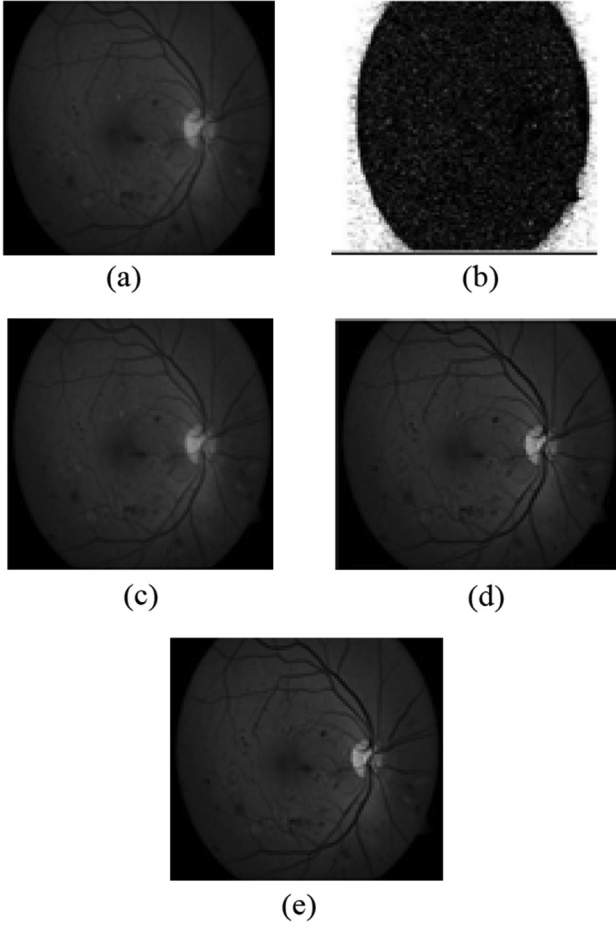
Fig. 3. (a) Green channel image (b) Regional minima image (c) Reconstructed image (d) Enhanced image (e) Smoothed image.

where b is structuring element.

3.2. Detection of blood vessels using iterative morphological approach

Green channel of RGB image is preferred for detection in blood vessel from the fundus image as shown in Fig. 3(a).

The main idea is the identification of foreground and background. We assume foreground as high intensity structures like optic disc and exudates, and background as low intensity structures like MAs, hemorrhages, and blood vessels. Background estimation has been accomplished using Regional Minima (RMIN) operator which emphasize the regional minima pixel, followed by reconstruction by dilation. By identifying the regional minima, the bright area, such as exudates are removed from the green channel image. Bright lesions are segmented from resulting image I_1 as shown by Eq. (7).

$$I_1 = R_{I_g}(RMIN(I_g)) \tag{7}$$

where $RMIN(I_g) = R*_{I_g}(I_g + 1)$ and $R_{I_g}(RMIN(I_g))$ are reconstruction by dilation using I_g as mask image and $RMIN(I_g)$ as marker image. $R*_{I_g}(I_g + 1)$ is gray scale reconstruction by erosion using I_g as mask and $(I_g + 1)$ as marker image. The regional minima and reconstructed images are shown in Fig. 3(b) and (c) respectively [24].

Now morphological contrast enhancement method is applied on I_1 image is described by Eq. (8)

$$I_2 = I_1 + \alpha_{th}(I_1) - \beta_{th}(I_1) \tag{8}$$

where $\alpha_{th}(I_1)$ is top hat by opening which contains only high intensity regions of I_1 and $\beta_{th}(I_1)$ is top hat by closing which contains low intensity regions. Then summing up the actual image with top hat

opening α_{th} and subtracting top hat by closing β_{th}, the enhancement of bright constituents are procured. Here ball shaped structuring element with 12-pixel radius and reference height of gray level is used. Enhanced image is shown in Fig. 3(d). Then Butter-worth Low Pass filter of order one is employed to diminish the impact of noise and MAs in detection process. The Butterworth filter of order one is defined by Eq. (9). Now, this filter is applied to I_2 as described in Eq. (10). The resulting smoothed images is shown in Fig. 3(e).

$$H(u, v) = \frac{1}{1 + [D(u, v)/D_0]^2} \tag{9}$$

$$I_3 = I_2 * H(u, v) \tag{10}$$

Next, top-hat transform by closing is applied to enhance the low intensity structure. The low intensity region are blood vessels, MAs and hemorrhages. We enhance the local minima and obtain a binary mask with retinal vein. Top-hat by closing is performed on image I_3 with structuring element B according to Eq. (11). Here, B is diamond shaped structuring element bigger than the maximum thickness of blood vessels. Here diamond shape structuring element with side of 14 pixels has been considered.

$$I_4 = \theta_{TH}^{(B)}(I_3) \tag{11}$$

Now *supremum of opening* of I_4 is calculated by set of linear structuring element. In this work 24 linear structuring elements are used with 100 pixels length. Linear structuring element is mapped to suit the foremost vessels in right and left eyes [27].

$$I_5 = \bigcup_{R_\phi=1}^{12} \alpha^{B_{R\phi}}(I_4) \bigcup_{L_\theta=1}^{12} \alpha^{B_{L\theta}}(I_4) \tag{12}$$

where $B_{R\Phi}$ is the structuring element utilized to recognise the superior and inferior of right eye and employed angle of gyration.

$$R_\phi = [15 \quad 30 \quad . \quad . \quad 90 \quad , \quad -15 \quad -30 \quad . \quad . \quad -90] \tag{13}$$

$B_{L\Phi}$ is the structuring element employed to the superior and inferior part of principal vein of left eye.

$$L_\phi = [105 \quad 120 \quad . \quad . \quad 180 \quad , \quad 195 \quad 210 \quad . \quad . \quad 270] \tag{14}$$

The resulting image of supremum of opening of right eye is shown in Fig. 4(b).

Now reconstruction by dilation is performed on supremum of opening in order to estimate the blood vessels. Reconstructed image of blood vessels is shown in Fig. 4(c).

$$I_6 = R_{I_4}(I_5) \tag{15}$$

where I_4 is mask image and I_5 is marker image. I_6 is gray scale image, it is binarized in which blood vessel pixels consist of 1 and remaining all pixels consist of 0. We binarise I_6 using thresholding technique. The pixel value greater than specified threshold is assigned 1 otherwise 0. The threshold is taken as 8; which has been determined by trial and error experiments. The blood vessels in binary image has been shown in Fig. 4(d).

Now these blood vessels have to be removed from fundus image. For this purpose, firstly CLAHE is applied on green channel image 5 (a) and resulting image is shown in Fig. 5 (b). Green channel CLAHE image was chosen because it has the highest contrast of the blood vessels [21].

$$I_7 = CLAHE(I_g) \tag{16}$$

Further, ASF is performed on CLAHE image (I_7). This is based on successive applications of morphological openings and closings. A disc-shaped structuring element B with radius of 15 pixels was used for this purpose. ASF resulting image is shown in Fig. 5(c). Now CLAHE image (I_7) is subtracted from ASF image (I_8), which is shown in Fig. 5(d).

$$I_8 = \varphi^s(\gamma^s(I_7)) \tag{17}$$

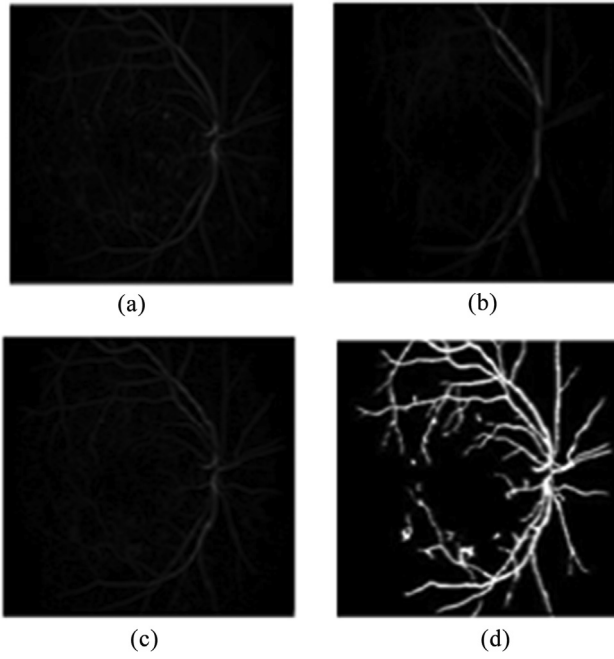$$\{I_9\} = \{I_8\} - \{I_7\} \tag{18}$$

Fig. 4. (a) Top-hat by closing image (b) Supremum of opening image (c) Reconstructed image (d) Blood vessels in binary image.

H-MINIMA (H_{min}) transform is applied on I_9 image in order to eliminate the regions with low contrast in image I_9. They could be optic disc or exudates. H_{min} transform eliminates the connected components with contrast less than specified threshold. The resulting image of H_{min} transform is shown in Fig. 5(e).

$$I_{10} = H\min(I_9) \tag{19}$$

Finally, regional minima (RMIN) operator is applied on resulting image I_{10}. RMIN operator based on morphological reconstruction by erosion, which converts the grayscale image into binary image without using any threshold. The pixel value of I_{11} is inverted as shown in Fig. 5(f).

$$I_{11} = RMIN(I_{10}) \tag{20}$$

Now blood vessel removal is achieved by subtracting the binary blood vessel image I_6 from RMIN operator image I_{11}. Some of the blood vessels residues are left in the eye image I_{12} which is shown in Fig. 6(a). The above morphological operation steps are applied on the remaining blood vessels residues. Residues after one more iteration are shown in Fig. 6(b). After comparing Fig. 6(a) and (b), it is clearly observed that improved blood vessels removal is achieved after one more iteration of blood vessel segmentation process.

$$I_{12} = imsubtract(I_{11}, I_6) \tag{21}$$

The steps for the detection of blood vessels are summarized below:

Step 1. Extract green channel from color fundus image.
Step II. Apply regional minima on green channel image.
Step III. Perform reconstruction by dilation regional minima image.
Step IV. Contrast enhancement is accomplished by morphological operator and followed by smoothing.
Step V. Perform top-hat transform by closing.
Step VI. Apply 24 times morphology opening on I_4 image with 15° rotation from vertical.
Step VII. Perform morphology reconstruction by dilation.
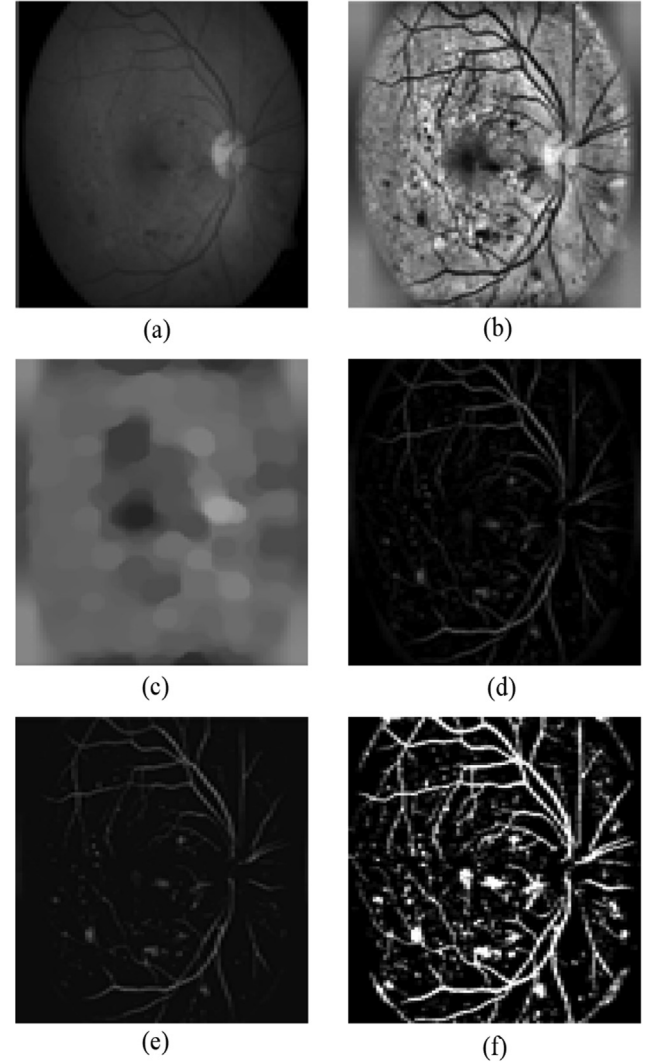Step VIII. Apply regional minimum operator and binaries it.

Fig. 5. (a) Green channel image (b) CLAHE image (c) ASF image (d) I_9 image (e) H_{min} operator image (f) Regional minima image.
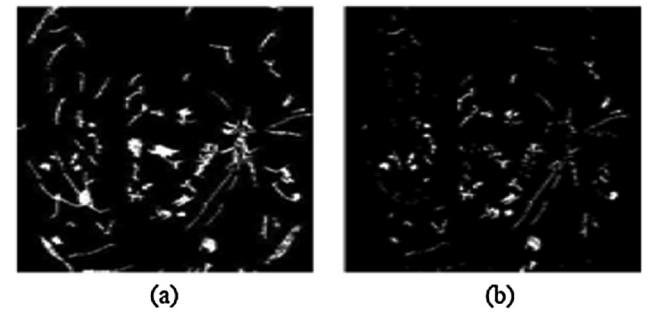

Fig. 6. (a) Residue after first time removal of blood vessels (b) Residue after one more iteration of removal algorithm of blood vessels.

3.3. Optic disc localization by Watershed segmentation method

Segmentation of optic disc plays essential role in detection of red lesions because some of the hemorrhages are very similar in size and color of optic disc. We have used Watershed Transform (WT) controlled with markers for optic disc segmentation from fundus photograph. The watershed transform is one of the methods in area of topography, widely used for morphological segmentation. It is marker based segmentation. Once marker is extracted precisely, segmentation can be

achieved correctly [28]. Watershed transform is fast, simple and intuitive method. It efficiently combines elements from similarity and discontinuity based methods. Conventional edge based methods most frequently form disconnected boundaries that need post-processing to produce closed regions. Watershed transform provides closed contour and it requires low computation time. It is able to accomplish complete partition of the image. Watershed algorithm is developed originally with grey scale image; hence it can be applied directly on pre-processed grey scale fundus image. WT for optic disc segmentation consists of many steps such as morphological gradient, marker-controlled watershed segmentation, erosion-based gray-scale image reconstruction, dilation -based gray-scale image reconstruction.

Morphological Gradient (MG): The gray scale image is changed into gradient image that specifies boundary quality of pixel. Limit is set with a specific goal, in order to convert every pixel to the edge point or non-edge point. A multiscale gradient algorithm is applied in order to achieve greater robustness to noise. The term multiscale refers to inspection of the images with different size structuring elements. The integration of MG in different scales, has strong tolerance to noise and it extracts a verity of fineness of the boundaries [25].

$$MG(I) = (I \oplus b) - (I \ominus b) \tag{22}$$

where I is gray scale image and b is disc structuring element with 3 pixel radius.

Marker-controlled Watershed Segmentation: The marker controlled watershed transform is powerful and open-ended method for sectionalisation of entity with secured outlines. This method is very effective to reduce the over segmentation of gray scale image, if one knows how to place marker inside the image. The marker image employed in watershed segmentation is a binary image containing isolated points or large regions, where every attached marker is situated inside the object of concern. Every marker has coordinated relationship to watershed areas, henceforth, the quantity of markers will be equivalent to the last bit of watershed area [25].

After calculating morphological gradient of gray scale image, next step is creating internal (foreground) marker and external (background) marker. We used erosion-based gray scale image reconstruction followed by dilation-based gray scale reconstruction. the result is shown in Fig. 7(c).

Erosion-based gray-scale image reconstruction [17]

The morphological reconstruction of I_8 from the marker f with short flat structuring element D, is represented as

$$I_8 \Delta_D f = (f \ominus_{I_8} D)^\infty \tag{23}$$

where $(f \ominus_{I_8} D) = (f \ominus D) \vee I_8$ is called conditional (geodesic) erosion. Now the n conditional erosion

$$(f \ominus_{I_8} D)^n = ((((f \ominus_{I_8} D) \ominus_{I_8} D) \ominus_{I_8} D) \ominus_{I_8}. \ldots \ominus_{I_8} D) \tag{24}$$

Dilation-based gray scale reconstruction [17]

The morphological reconstruction of I_8 from the marker f with short flat structuring element D is

$$I_8 \Delta_D f = (f \oplus_{I_8} D)^\infty \tag{25}$$

where $(f \oplus_{I_8} D) = (f \oplus D) \wedge I_8$ is called conditional (geodesic) dilation. The n conditional dilations is given as.

$$(f \oplus_{I_8} D)^n = ((((f \oplus_{I_8} D) \oplus_{I_8} D) \oplus_{I_8} D) \oplus_{I_8}. \ldots \oplus_{I_8} D) \tag{26}$$

where $I_8 \Delta_D f$ is infinite reconstruction of I_8 from the marker f, using the connectivity given by the structuring element D. $I_8 \hat{} f$ is pixel wise *minimum* between two images. $I_8 \vee f$ is pixel wise *maximum* between two images.

In the next step, *regional maxima* are applied on resulting image. *Reconstruction by opening* will take place in order to create the internal marker. Internal marker is superimposed on original image. The external marker is created around the optic disc of predefined radius centre. The internal marker image and superimposed image are shown
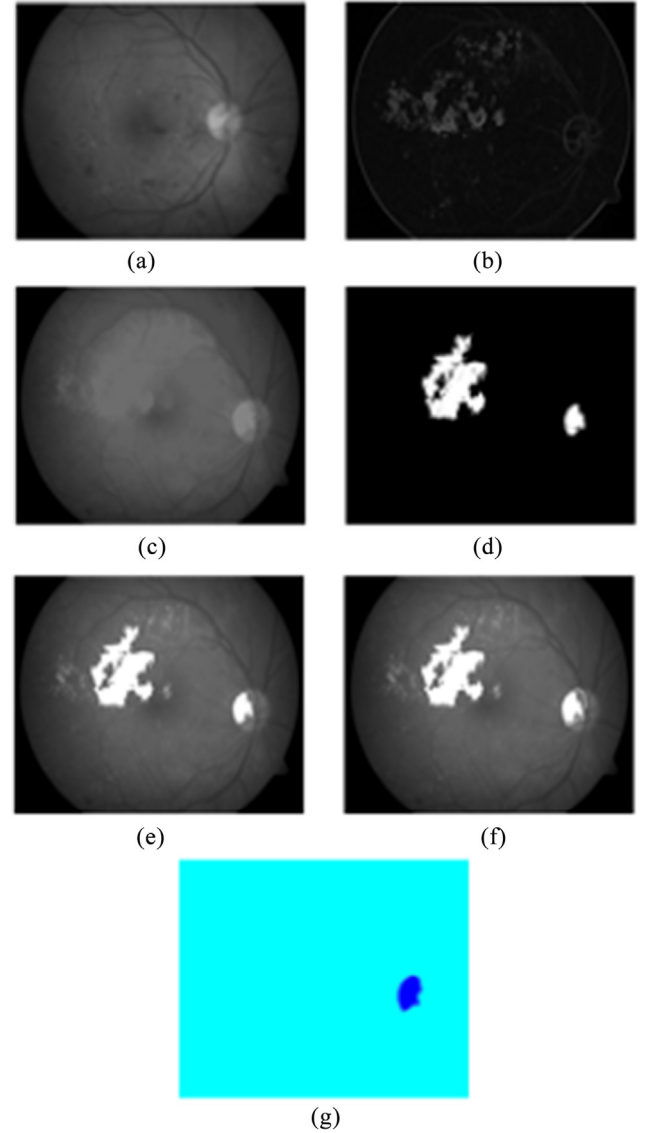

(a)

(b)

(c)

(d)

(e)

(f)

(g)

Fig. 7. (a) Gray scale image (b) Gradient image (c) Image after erosion based reconstruction followed by dilation based reconstruction (d) Regional maxima image (e) Regional maxima image superimposed on original image (f) Segmented optic disc (g) Segmented optic disc in coloured image.

on Fig. 7(d) and (e) respectively. Then watershed transform is applied on superimposed image for segmentation of optic disc. Only optic disc is segmented from grey scale image because of external marker. The optic disc is shown by watershed ridge lines in Fig. 7(f). Finally segmented optic disc in coloured image is shown in Fig. 7(g).

3.4. Fovea localization

Fovea is dark region inside the macula which is responsible for sharp central vision. Fovea has similar colour to some of DR lesions. It is difficult to differentiate fovea and some large haemorrhages, because of same colour. Hence, it is essential to segment fovea from the fundus image in order to detect diabetic retinopathy. Mathematical morphology is applied on gray scale image for fovea localization. Fovea extraction images are shown in Fig. 8.

The steps for detection of fovea are summarised as:

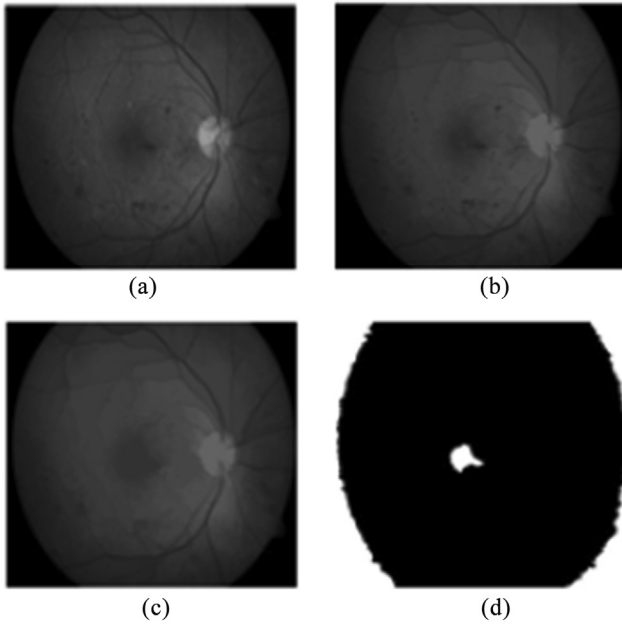Step I *Opening by reconstruction* is tested on grey scale image with disc shape structuring element.

Fig. 8. (a) Gray scale image (b) Opening by reconstruction image (c) Opening closing by reconstruction image (d) Segmented fovea image.

Step II *Closing by reconstruction* is tested on resulting image of opening by reconstruction. These operations create the flat minima inside the image.

Step III Regional minima are applied on opening closing reconstruction image and erosion is performed on the resulting image with disc shape structuring element.

Now all the pathological structures, namely vascular tree, optic disc and fovea which may cause false positive, are removed from the fundus image. The remaining pathological structures are microaneurysm and haemorrhages. Extracted haemorrhages and MAs from colour fundus image are shown in Fig. 9.

3.5. Feature extraction of micoaneurysm and hemorrhages

After extracting microaneurysms and hemorrhages from fundus image, feature selection takes place in order to acquire relevant information from the given image. Since hemorrhages have particular properties, for example, round shape and red shading [29,30]. Feature extraction is very useful in artificial intelligence. The parameters of radial basis function neural network are trained by the features of the MAs and hemorrhages. Features such as area, perimeter, circularity,
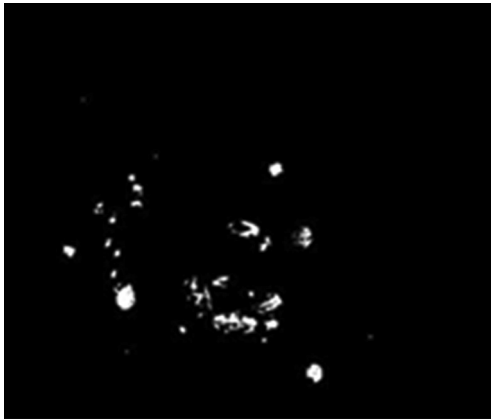
Fig. 9. Extracted MAs and hemorrhages.

number of lesions, major axis length, minor axis length, and aspect ratio have been extracted [31,32]. Enhanced robustness of the proposed DR detection model is achieved by extracting more number of relevant features. Extracted features of MAs and hemorrhages, and their descriptions are shown in Table 1.

3.6. Classification of diabetic retinopathy using radial basis function neural network (RBF NN) [33]

RBF is a special case of single-hidden layer neural network for application to problems of supervised learning which is widely used for classification and regression. The model of RBF neural network is shown in Fig. 10. Radial Basis Function NN is a three-layer network, including input and output layer. Therefore, design of RBF NN is much simpler as compared to many other classifiers. Since, it has only one hidden layer, computational complexity of RBF classifier is lesser than feed forward NN based classifiers. RBF NN has strong tolerance to input noise, and online learning ability. Further, RBFNN has very good generalization properties. The properties of RBF networks make it very suitable to regression model as well as classification. The expression of RBFNN model with K centres, is described by Eq. (27). The network consists of three parameters, namely- output layer weights, centres and standard deviation. Output layer weights are linear parameters that regulate the height of the basis function and hence, RBFNN is known as linear model. Centres are non-linear parameters of the unrevealing layer neurons, regulate the location of the basis function. Standard deviation is nonlinear parameter of the hidden layer. It dictates the spread of the basis function. The number of centres regulate the architecture model because the number of neurons in hidden layer is equivalent to the number of centre. These all three parameters of network would be trained by the features extracted from the MAs and hemorrhages.

$$F(x) = \sum_{k=1}^{K} w_k \exp\left(-\frac{\|x_n - \mu_k\|^2}{\sigma_k^2}\right) \tag{27}$$

It is rewritten as

$$F(x) = \sum_{k=1}^{K} w_k \phi_k \tag{28}$$

where $\phi(x) = \exp\left(-\frac{\|x_n - \mu_k\|^2}{\sigma_k^2}\right)$

Choosing the centres: The centres of network are chosen by K-mean clustering. It iteratively minimizes the distance between data and centres as described in Eq. (29). K-mean clustering is an example of unsupervised learning. Lloyd algorithm for convergence of centre at local minima is described by the Eqs. (30) and (31) [34,35].

Iteratively minimized the objective function

$$\sum_{k=1}^{K} \sum_{x_n \in s_n} \|x_n - \mu_k\|^2 \tag{29}$$

with respect to S_K and μ_K. update centre (μ_K) and cluster (S_K)

$$\mu_k \leftarrow \frac{1}{|S_k|} \sum_{x_n \in s_k} x_n \tag{30}$$

$$S_k \leftarrow \{x_n: \|x_n - \mu_k\| \leqslant all \ \|x_n - \mu_k\|\} \tag{31}$$

Finally, the Lloyd algorithm converges into local minima and optimum centres are achieved.

Choosing the weight: RBF network with *K* centres has been chosen for classification. The number of inputs are more than the number of weights of the network, as shown in Eq. (32). The number of input indicates the number of equations, which are more than number of unknowns (weights). Such systems are called as *over determined* systems, which do not have exact solution. Therefore, we go for the approximate solution by applying *Least Square* or *Pseudo Inverse* methods.

Table 1
Extracted features of MAs and hemorrhages for proposed DR detection.

Feature	Description
Area of object	The aggregate number of pixel in the area
Perimeter of object	Add up all the pixels on perimeter of object
Circularity	Roundness of the candidate
Number of objects	Total number of discontinuity in the region
Major axis length of the candidates	Total length of the major axis of the ellipse that has the identical normalized second central moment of the zone
Minor axis length of the candidates	Total length of the minor axis of the ellipse of the identical normalised second central moment of the region
Aspect ratio	Ratio of major axis length and minor axis length
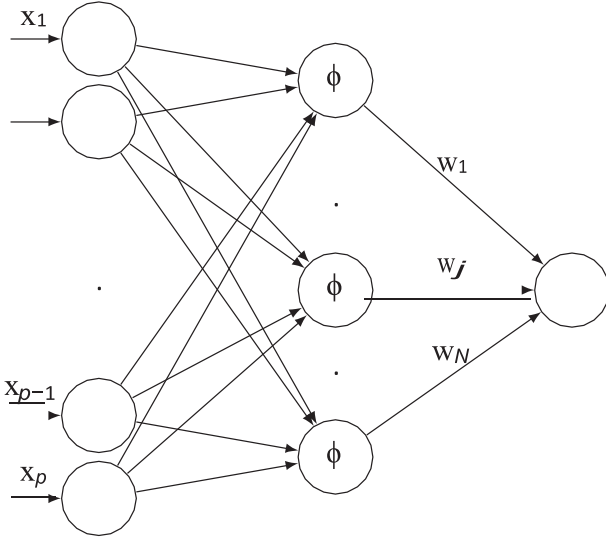
Fig. 10. RBF NN model.

Least square solution minimizes the addition of all of the squares of errors produced in the result of each isolated equation. The solution of least square problem is achieved by normal equation, which is described in Eq. (33) [29,30].

$$y_n \approx \sum_{k=1}^{K} w_k \exp\left(-\frac{\|x_n - \mu_k\|^2}{\sigma_k^2}\right)$$

(32)

N equation in $K \ll N$ unknowns. If $\phi^T\phi$ is invertible

$$w = [\phi^T\phi]^{-1}\phi^T y$$

(33)

Standard deviation (σ) is calculated using back propagation algorithm. The number and dimension of standard deviation (σ) are same as centres of the neural network. In this work, we have chosen eight centres, which are determined by trial and error method. Hence, the number of neurons in hidden layer are eight. The parameters of RBF network are trained by considering extracted features (Table 1) as *input* and *class* as output. Here, binary classification (DR and healthy) has been performed for the detection of DR.

4. Results

The results of proposed DR detection model from fundus image have been discussed in details in this section. The accuracy of result obtained from the suggested DR detection algorithm is based on evaluated sensitivity and specificity. One hundred thirty images (Healthy and DR images) have been taken from DIABET DB1 and Diaretdb0 v 1 1 database. Out of these, sixty seven eye images have been used as training samples and sixty three images as testing samples. Number of samples in training set and test set are chosen randomly, which provides robustness to the proposed algorithm. The number of training samples are chosen more than the test samples, for better training of classification model. Table 2 shows the retinal fundus images under investigation and

the corresponding output images containing MAs and hemorrhages along with some blood vessel residues. RBFNN based classifier used in the proposed work, classifies as 'DR' and 'healthy' images. For the validation of the diagnostic results obtained from the proposed DR detection system, diagnostic opinion has been obtained from ophthalmologist. Comparison table of proposed method and ophthalmologist opinion is shown in Table 3. In this table, inference generated by proposed method and inference drawn by ophthalmologist are shown. Table 3 infers that proposed method has very good match with ophthalmologist opinion for early detection of DR. Out of 10 images investigated during the experiment, 6 were DR affected and 4 were healthy eyes. It is observed that DR affected retinal fundus image contains nearly circled bright spots namely- haemorrhages & MAs, and some blood vessels residues. However, in case of healthy eye fundus image, only some vascular residues are present.

The number of true positive, true negative, false positive and false negative of the proposed DR detection method are twenty nine, twenty eight, four and two respectively. The sensitivity and specificity of proposed system have been computed as 87% and 93% respectively. The obtained results of the proposed method are compared with some existing methods. The comparison is shown in Table 4, which states that the proposed method is better than the considered existing methods.

5. Conclusion

This paper presented a scheme for the early detection of DR from colour fundus image for abundance screening of DR. The achieved values of sensitivity and specificity show that the proposed diagnostic system is better for non-proliferative diabetic retinopathy detection. The DR detection model was trained by seven features of haemorrhages and MAs, which made the proposed system robust and reliable. Future work of this paper is to propose a proliferative diabetic retinopathy detection system by considering cotton wools and abnormal blood vessels from colour fundus images. DR detection system could be extended to multi class diabetic retinopathy classification, to classify into healthy, mild NDPR, moderate NDPR, severe NDPR, and PDR. For classification, Feed Forward Neural Network, Probabilistic Neural Network (PNN), SVM and other emerging models can be examined.
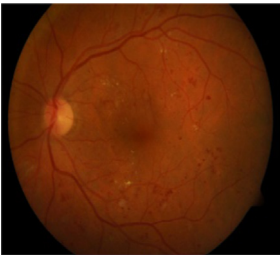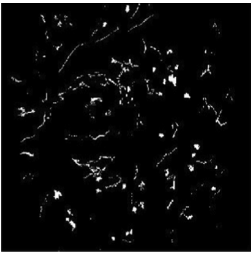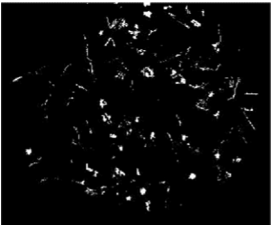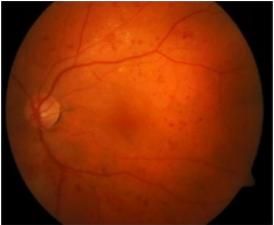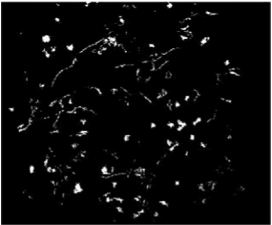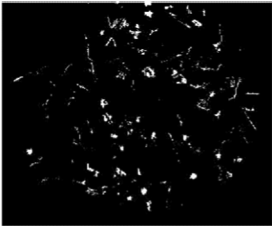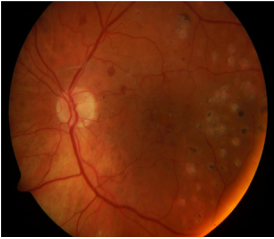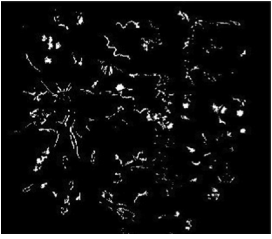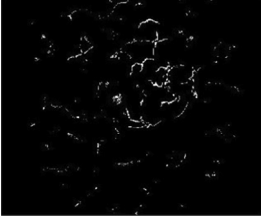
Appendix A. Supplementary material

Supplementary data to this article can be found online at https://doi.org/10.1016/j.optlastec.2019.105815.

Table 2
Fundus image and corresponding output.

S. No	Fundus Image	Extracted MAs and Hemorrhages
1		
2		
3		
4		
5		
6		
7		

Table 2 (*continued*)
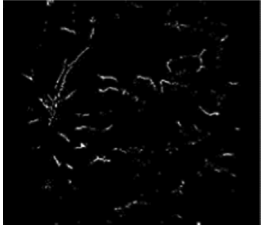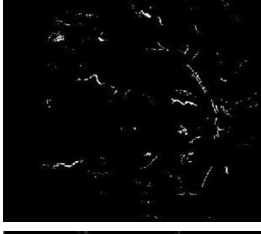
S. No	Fundus Image	Extracted MAs and Hemorrhages
8		
9		
10		

Table 3
Comparison of the diagnostic conclusion made by the proposed system and ophthalmologist opinion.

S. No	Diagnostic decision based on features presence			
	Microaneurysm	Hemorrhages	Inference generated by proposed scheme	Inference drawn by ophthalmologist	
1	Yes	Yes	DR presence	MAs, Hemorrhages	DR presence
2	Yes	Yes	DR presence	MAs, Hemorrhages, exudate	DR presence
3	Yes	Yes	DR presence	MAs, Hemorrhages, exudates and cotton wools	DR presence
4	Yes	Yes	DR presence	MAs, Hemorrhages, exudate	DR presence
5	Yes	Yes	DR presence	MAs, Hemorrhages, exudate and cotton wools	DR presence
6	Yes	Yes	DR presence	MAs, Hemorrhages	DR presence
7	Yes	Yes	DR presence	Hemorrhages, lasers	DR presence
8	No	No	DR absence	Healthy eye	DR absence
9	No	No	DR absence	Healthy eye	DR absence
10	No	N0	DR absence	Healthy eye	DR absence

Table 4
Comparison result of proposed method with existing method.

	Sensitivity	Specificity
Kedir M. Adal et al. [6]	81.08%	92.3%
J.P. Bea et al. [9]	82.9%	
S. S. Rahim et al. [2]	80%	55%
Proposed Method	87%	93%

References

[1] S.B. Junior, D. Welfer, Automatic detection of microaneurysms and hemorrhages in color eye fundus images, Int. J. Comp. Sci. Inform. Technol. 5 (5) (2013) 21.

[2] S.S. Rahim, C. Jayne, V. Palade, J. Shuttleworth, Automatic detection of microaneurysms in colour fundus images for diabetic retinopathy screening, Neural Comput. Appl. 27 (5) (2016) 1149–1164.

[3] Meindert Niemeijer, Bram Van Ginneken, Michael J. Cree, Atsushi Mizutani, Gwénolé Quellec, Clara I. Sánchez, Bob Zhang, et al., Retinopathy online challenge: automatic detection of microaneurysms in digital color fundus photographs, IEEE Trans. Med. Imaging 29 (1) (2009) 185–195.

[4] D. Marin, M.E. Gegundez-Arias, A. Suero, J.M. Bravo, Obtaining optic disc center and pixel region by automatic thresholding methods on morphologically processed fundus images, Comput. Methods Programs Biomed. 118 (2) (2015) 173–185.

[5] S.S. Rahim, V. Palade, J. Shuttleworth, C. Jayne, Automatic screening and classification of diabetic retinopathy fundus images, International Conference on Engineering Applications of Neural Networks, Springer, 2014, pp. 113–122.

[6] Kedir M. Adal, Désiré Sidibé, Sharib Ali, Edward Chaum, Thomas P. Karnowski, Fabrice Mériaudeau, Automated detection of microaneurysms using scale-adapted blob analysis and semi-supervised learning, Comput. Methods Programs Biomed. 114 (1) (2014) 1–10, https://doi.org/10.1016/j.cmpb.2013.12.009.

[7] R. Inbarathi, R. Karthikeyan, Detection of retinal hemorrhage in fundus images by classifying the splat features using svm, Int. J. Innov. Res. Sci., Eng. Technol. 3 (2014) 1979–1986.

[8] P. Jitpakdee, P. Aimmanee, B. Uyyanonvara, A survey on hem- orrhage detection in diabetic retinopathy retinal images, 2012 9th International Conference on Electrical Engineering/Electronics, Computer, Telecommunications and Informa- tion Technology (ECTI-CON), IEEE, 2012, pp. 1–4.

[9] J.P. Bae, K.G. Kim, H.C. Kang, C.B. Jeong, K.H. Park, J.M. Hwang, A study on hemorrhage detection using hybrid method in fundus images, J. Digit. Imaging 24 (3) (2011) 394–404.

[10] A.D. Fleming, S. Philip, K.A. Goatman, J.A. Olson, P.F. Sharp, Automated microaneurysm detection using local contrast normalization and local vessel detection, IEEE Trans. Med. Imaging 25 (9) (2006) 1223–1232.

[11] S.S. Rahim, V. Palade, J. Shuttleworth, C. Jayne, Automatic screening and classification of diabetic retinopathy and maculopathy using fuzzy image processing, Brain Informatics 3 (4) (2016) 249–267.

[12] T. Walter, J.-C. Klein, P. Massin, A. Erginay, A contribution of image processing to the diagnosis of diabetic retinopathy-detection of exudates in color fundus images of the human retina, IEEE Trans. Med. Imaging 21 (10) (2002) 1236–1243.

[13] R.P. Danis, M.D. Davis, Proliferative diabetic retinopathy, Springer, 2008, pp. 29–65.

[14] K.B. Shah, D.P. Han, Proliferative diabetic retinopathy, Int. Ophthalmol. Clinics 44 (4) (2004) 69–84.

[15] R. Welikala, J. Dehmeshki, A. Hoppe, V. Tah, S. Mann, T.H. Williamson, S. Barman, Automated detection of proliferative dia- betic retinopathy using a modified line operator and dual classification, Comput. Methods Programs Biomed. 114 (3) (2014) 247–261.

[16] D.R.S.R. Group, et al., Photocoagulation treatment of proliferative diabetic retino-pathy: clinical application of diabetic retinopathy study (drs) findings, drs report number 8, Ophthalmology 88 (7) (1981) 583–600.

[17] E.R. Dougherty, R.A. Lotufo, Hands-on Morphological Image Processing, SPIE press, 2003.

[18] J. Serra, P. Soille, Mathematical Morphology and its Applications to Image Processing, Springer Science & Business Media, 2012.

[19] R. Radha, B. Lakshman, Identification of retinal image features using bitplane se-paration and mathematical morphology, 2014 World Congress on Computing and Communication Technologies (WCCCT), IEEE, 2014, pp. 120–123.

[20] S.H. Rasta, M.E. Partovi, H. Seyedarabi, A. Javadzadeh, A com- parative study on preprocessing techniques in diabetic retinopathy retinal images: illumination cor-rection and contrast enhancement, J. Med. Signals Sensors 5 (1) (2015) 40.

[21] S.K. Yadav, S. Kumar, B. Kumar, R. Gupta, Comparative analysis of fundus image enhancement in detection of diabetic retinopathy, 2016 IEEE Region 10 Humanitarian Technology Conference (R10-HTC), IEEE, 2016, pp. 1–5.

[22] V. Thirilogasundari, S.A. Janet, et al., Fuzzy based salt and pepper noise removal using adaptive switching median filter, Procedia Eng. 38 (2012) 2858–2865.

[23] A. Hussain, M. Habib, A new cluster based adaptive fuzzy switching median filter for impulse noise removal, Multimedia Tools Appl. 76 (21) (2017) pp. 22 001–22 018.

[24] D. Welfer, J. Scharcanski, C.M. Kitamura, M.M. Dal Pizzol, L.W. Ludwig, D.R. Marinho, Segmentation of the optic disk in color eye fundus images using an adaptive morphological approach, Comput. Biol. Med. 40 (2) (2010) 124–137.

[25] K. Parvati, P. Rao, M. Mariya Das, Image segmentation using gray- scale mor-phology and marker-controlled watershed transformation, Discrete Dynamics Nature Soc. 2008 (2008).

[26] S. Kumar, B. Kumar, Diabetic retinopathy detection by extracting area and number of microaneurysm from colour fundus image, 2018 5th International Conference on Signal Processing and Integrated Networks (SPIN), IEEE, 2018, pp. 359–364.

[27] E. Ricci, R. Perfetti, Retinal blood vessel segmentation using line operators and support vector classification, IEEE Trans. Med. Imaging 26 (10) (2007) 1357–1365.

[28] Niket Amoda, Ramesh K. Kulkarni, Efficient Image Segmentation Using Watershed Transform, Int. J. Comp. Sci. Technol. (IJCST) iv (ii), ver 2.

[29] Lama Seoud, Thomas Hurtut, Jihed Chelbi, Farida Cheriet, J.M. Pierre Langlois, Red lesion detection using dynamic shape features for diabetic retinopathy screening, IEEE Trans. Med. Imaging 35 (4) (2016) 1116–1126.

[30] Behdad Dashtbozorg, Jiong Zhang, Fan Huang, M. Bart ter Haar Romeny, Retinal microaneurysms detection using local convergence index features, IEEE Trans. Image Process. 27 (7) (2018) 3300–3315.

[31] Wen Cao, Nicholas Czarnek, Juan Shan, Lin Li, Microaneurysm detection using principal component analysis and machine learning methods, IEEE Trans. Nanobiosci. 17 (3) (2018) 191–198.

[32] Ramon Pires, Sandra Avila, Herbert F. Jelinek, Jacques Wainer, Eduardo Valle, Anderson Rocha, Beyond lesion-based diabetic retinopathy: a direct approach for referral, IEEE J. Biomed. Health. Inf. 21 (1) (2017) 193–200.

[33] O. Nelles, Nonlinear system identification: from classical approaches to neural networks and fuzzy models, Springer Science & Business Media, 2013.

[34] R.S. Michalski, J.G. Carbonell, T.M. Mitchell, Machine learning: An artificial in-telligence approach, Springer Science & Business Media, 2013.

[35] C.M. Bishop, et al., Neural Networks for Pattern Recognition, Oxford University Press, 1995.